# Examining the quality of CFOSAT-based surface winds over global oceans with respect to 111 buoys

**Yuxin Liu[1, 2, 3], Xiangzhou Song[1, 3†], Changsan Xu[1, 3], Chunlin Ning[4], Yongliang Duan[4], Shilin Tang[5], Mingsen Lin[2, 6] and Xingwei Jiang[2, 5]**

[1] Key Laboratory of Marine Hazards Forecasting, Ministry of Natural Resources (MNR), Hohai University, Nanjing, China;

[2] National Satellite Ocean Application Service, MNR, Beijing, China;

[3] College of Oceanography, Hohai University, Nanjing, China;

[4] First Institute of Oceanography, MNR, Qingdao, China;

[5] State Key Laboratory of Tropical Oceanography, South China Sea Institute of Oceanology, Chinese Academy of Sciences, Guangzhou, China;

[6] Key Laboratory of Space Ocean Remote Sensing and Application, MNR, Beijing, China.

Corresponding author: Xiangzhou Song (xzsong@hhu.edu.cn)

†1 Xikang Road, Hohai University, Nanjing, China.

**Key Points:**

- The global sea surface wind vector products from the China-France Oceanography Satellite are validated and compared to buoy observations.
- The root mean square errors of wind speed and wind direction were 1.1 $ms^{-1}$ and 20.4° at the global scale, respectively.
- The wind quality in the subtropics is slightly higher than that in the tropics at the designed observational accuracy.

## Abstract

The China-France Oceanography Satellite (CFOSAT), launched on 29 October 2018, is the world's first satellite that carries both a real aperture radar spectrometer and a fan-shaped beam rotary scanning scatterometer. This study examined the retrieval results for the scatterometer onboard the CFOSAT with respect to global buoys from NDBC, TAO/TRITON, PIRATA, RAMA, PMEL, and MNR in 2019. For the scatterometer products in the range of 4-24 $ms^{-1}$, the root-mean-square error (RMSE) of the wind speed was 1.1 $ms^{-1}$, and the wind direction RMSE was 20.4° at the global scale. In the tropics, the wind speed and wind direction RMSEs were 1.1 $ms^{-1}$ and 21.5°, respectively, while the corresponding RMSEs decreased to 1.1 $ms^{-1}$ and 18.8° in the subtropics. The error statistics were larger in the range of 0-4 $ms^{-1}$, which is beyond the designed measurement accuracy, and the wind speed was overestimated. Overall, the CFOSAT measurements are reliable in the range of 4-24 $ms^{-1}$, thus meeting the accuracy requirements of the technical design. Finally, the influence of surface currents on the CFOSAT measurements was analyzed. The results indicate that the differences between the CFOSAT measurements and buoy observations in the tropics were reduced by excluding the effect of the surface currents.

## Plain Language Summary

A special collection presents new results on various topics for the ‘China-France Oceanography Satellite (CFOSAT): Scientific Applications’; however, the quality of satellite data should be examined before scientific use. Using 111 *in situ* moored buoys over the global ocean, new wind measurements based on CFOSAT are validated in this paper to provide uncertainty information for future users. In general, within the designed wind speed range of 4-24 $ms^{-1}$, CFOSAT wind speed and direction observations meet the designed accuracy requirements. However, when the wind speed is in the range of less than 4 $ms^{-1}$, which exceeds the designed measurement range, the error statistics are larger. The results indicate that the quality of satellite observations is different between tropical and subtropical regions, and the quality of CFOSAT winds in tropical regions is slightly lower than that in subtropical regions. In addition, this study shows that the influence of surface currents on the CFOSAT sea surface winds in the tropics cannot be ignored. The validated measurement results will be helpful for future wind products and studies of air-sea interactions and provide an effective error reference for future scientific applications of CFOSAT users.

## 1 Introduction

Sea surface wind is one of the key essential ocean and climate variables (EOCVs) for the study of air-sea interactions and climate change. It can be used to estimate the momentum and heat fluxes between the ocean and the atmosphere and to determine multiscale ocean dynamics in terms of the Langmuir circulation (Thorpe, 2004), surface Ekman currents and transport (Ekman, 1905; Price et al., 1987), mixed layer evolution (Pollard et al., 1973; Price et al., 1986), large-scale ocean circulations associated with Ekman pumping (Pedlosky, 1987; Huang, 2010), coastal upwelling, and oceanic/atmospheric coupling associated with both tropical instability waves and ocean fronts, as well as for forecasting the weather, waves and storm surges (Pollard et al., 1973; Price et al., 1986). In addition to driving physical processes in the upper ocean, winds are vital for studies of biogeochemical cycles within the ocean; for example, the air-sea flux of carbon dioxide (CO2) is closely related to the surface wind speed (Wanninkhof, 1992; Wanninkhof & Mcgillis, 1999). Surface winds are also used to provide observations of sea ice extent and rainfall (Bourassa et al., 2009). Thus, they can play an important role in driving ocean dynamic processes and modulating air-sea heat flux, moisture flux and gas flux. Accurate estimates of surface winds hold great importance for atmospheric and oceanic processes, which are valuable for marine engineering, disaster prevention and mitigation, resource assessment, climate change, etc.

Surface winds can be measured using *in situ* techniques, e.g., the global tropical moored buoy array or remote sensing instruments (e.g., scatterometer), such as NASA's Ku-band QuikSCAT and ESA's C-band ASCAT. A buoy can observe the surface winds directly by means of different types of anemometers; however, a satellite infers the winds at a normal height of 10 m through the radar energy reflection by recognizing the sea surface roughness. Therefore, satellite-derived wind data should be validated with respect to buoy observations before analysis or even the production of satellite-blended datasets (Atlas et al., 2011). In addition to traditional buoys, wave glider wind observations with a flexible strategy can be a powerful new way to identify potential errors in satellite observations (Schmidt et al., 2017; Liu, Y et al., 2021).

Global sea surface wind observations have been possible since the launch of the Seasat-A Satellite Scatterometer (SASS) on the NASA Seasat-A satellite (SEASAT-A) in June 1978. Over the next 40 years, a number of satellites equipped with observation sensors were launched, which not only used scatterometers but also used passive microwave radiometers, synthetic aperture radar and passively polarized microwave radiometers (Bourassa et al., 2009; Yu, L & Jin, 2012). The Chinese-French scatterometer (CSCAT) onboard the Chinese-French Oceanic Satellite (CFOSAT) is one of the communities and can be used for observation research and marine meteorological forecasting to improve the accuracy and timeliness of forecasting disastrous sea conditions such as tropical storms, storm surges and giant waves (NSOAS, http://www.nsoas.org.cn/eng). A recent study analyzed the global spatial distribution of wave-induced stress and its correlated index using simultaneous ocean surface winds and wave spectra from CFOSAT (Chen et al., 2020). Through fusion and processing with other sea surface wind data, global merged wind products with high spatial and temporal resolutions, such as cross-calibrated multiplatform (CCMP) wind vector analysis, can be generated to meet higher requirements.

Evaluation is required before the utilization of satellite observations to clarify the reliabilities and characteristics of measurements. Numerous evaluations of a series of scatterometers, such as the Seasat-A/SASS, the Active Microwave Instrument on the European Remote Sensing Satellite (ERS/AMI), the Advanced Earth Observing Satellite (ADEOS/NSCAT), the Quik Scatterometer (QSCAT/SeaWinds), the Meteorological Operational Satellite Programme Advanced Scatterometer (MetOp/ASCAT), the Oceansat Scatterometer (Oceansat/OSCAT) and the HaiYang-2 Scatterometer (HY-2/HYSCAT), have been carried out (Chelton et al., 1989; Bentamy et al., 1994; Bourassa et al., 1997; Ebuchi, 1999; Ebuchi et al., 2002; Chelton & Freilich, 2005; Zhao, X & Hou, 2006; Verspeek et al., 2010; Kumar et al., 2013; Zhao, K & Zhao, 2019; Wang, Z et al., 2020). Previous studies made pioneering contributions to the use of satellite-based wind products and quality control. The backscatter and wind quality were analyzed before launch based on the prototype of the CFOSAT simulator (Lin et al., 2019). However, the observational quality of surface vectors still needs to be examined compared to *in situ* measurements. Thus, the main purpose of this paper is to provide a thorough quality test for CSCAT wind data. In addition, another motivation for the validation is related to the influence of surface currents on the scatterometer observations. It should be noted that the errors may differ from those of traditional scatterometers due to a newly designed rotating fan-beam antenna. These differences are beyond the scope of the current study but will be investigated in future studies.

The remainder of this paper is organized as follows. In Section 2, the datasets, materials and methods are briefly introduced. The CSCAT data quality is validated compared to global buoy observations, and the influence of surface currents is explored in Section 3. Discussions based on the error statistics are presented in Section 4. Finally, conclusions of the CSCAT examinations are provided in Section 5.

## 2 Materials and Methods

### 2.1 Materials

CFOSAT carries two payloads: a surface wave investigation and monitoring (SWIM) system and a scatterometer, which realize the joint observation of sea waves and sea winds for the first time. The scatterometer measures the Bragg scattering of microwaves by capillary gravity waves caused by sea surface winds, and the sea surface scattering information with respect to the amplitude and texture direction of the capillary wave is retrieved using the National Aeronautics and Space Administration Scatterometer version 4 (NSCAT-4) Geophysical Model Function (GMF) to produce 10 m neutral equivalent winds (Xu et al., 2020; KNMI, https://scatterometer.knmi.nl/nscat_gmf). CSCAT is the first fan-beam rotary scatterometer in the world that can observe the same cell in a swath many times, obtaining abundant backscattering information to retrieve more accurate wind speed and wind direction (Wang, L et al., 2019). It works in the Ku-band and provides a swath of 1000 km. The Ku-band is sensitive to changes in wind speeds but is susceptible to rainfall. When the wind speeds are within the range of 4-24 $ms^{-1}$, the wind speed accuracy requirement is better than 2 $ms^{-1}$ (or 10% of the wind speed), and the wind direction accuracy requirement is better than 20° (NSOAS, http://www.nsoas.org.cn/eng).

The CSCAT products have two resolutions: 12.5×12.5 km and 25×25 km; the more common 25×25 km resolution spaceborne scatterometer product is selected in this study. Table 1 lists the main parameters of the CFOSAT (NSOAS, http://www.nsoas.org.cn/eng). The CFOSAT data were obtained from the Chinese National Satellite Ocean Application Service (NSOAS), ranging from January to December 2019. In this paper, the quality of the wind is examined and compared to the *in situ* buoy observations in the first calendar year (2019) after the CFOSAT was launched. The following sections show the discrepancies in wind information between the satellite retrievals and buoy observations for future users.

**Table 1.** Main Parameters of the CFOSAT (CSCAT).

| | |
|---|---|
| Orbit | ~520 km |
| Antenna beam shape | Fan pencil beam |
| Center frequency | 13.256 GHz (Ku-band) |
| Band width | 0.5 MHz |
| Swath width | ~1000 km |
| Polarizations | HH, VV |
| Incident angle | 26°-46° |
| Resolution | 12.5 km and 25 km |
| Measurement range | 4-24 $ms^{-1}$ |
| Accuracy | ± 2 $ms^{-1}$ or 10% for wind speed<br>± 20° for wind direction |

CSCAT was validated with respect to globally distributed buoys, including buoys from the US National Data Buoy Center, Tropical Ocean-Atmosphere/TRIangle Trans-Ocean buoy Network (TAO/TRITON), Prediction and Research Moored Array in the Tropical Atlantic (PIRATA), the Research Moored Array for African-Asian-Australian Monsoon Analysis and Prediction (RAMA) (Brocca et al., 2011), SF304 buoy and Nansha buoy affiliated with China's Ministry Natural Resources (MNR) (Liu, Y et al., 2021), the Bailong buoy belonging to the Indian Ocean Observing System (IndOOS), RAMA and MNR (Freitag et al., 2016; Feng et al., 2020), and the Kuroshio Extension Observatory (KEO) buoy and Papa buoy affiliated with the

NOAA/Pacific Marine Environmental Laboratory (PMEL). It should be noted that the traditional TAO/TRITON mission is under reconstruction as a modern, sustained tropical Pacific observation system within the context of the existing and planned Global Ocean Observing System (GOOS), which is called Tropical Pacific Observing System 2020 (TPOS 2020) (Kessler et al., 2019). Before the buoy observations in 2019 were selected, their offshore distances were calculated. Buoys with an offshore distance of more than 100 kilometers were excluded from this study to avoid potential uncertainties in the coastal regions for satellite measurements. Buoys were classified as tropical (23.5°S-23.5°N) or subtropical (23.5°N-60°N) according to their latitudes. A schematic diagram of the buoy locations and the CFOSAT trajectory is shown in Figure 1.

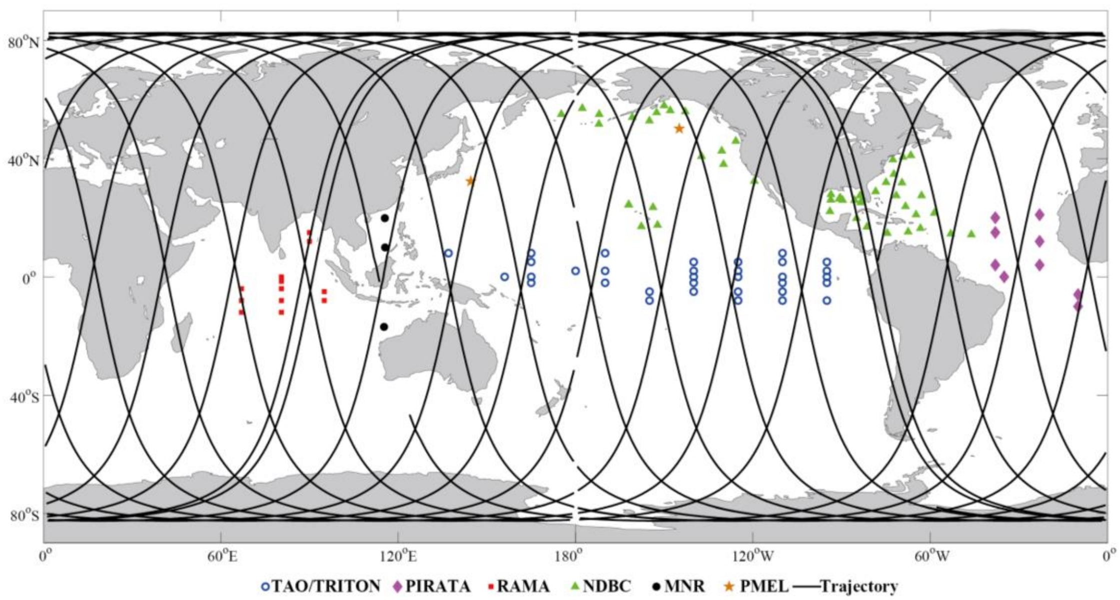


**Figure 1.** Schematic diagram of buoy locations used in this paper and the CFOSAT trajectory. Additional information can also be found in other studies (Chen et al., 2020). The buoys from TAO/TRITON, PIRATA, RAMA, NDBC, PMEL, and MNR (SF304, Bailong, and Nansha) are labeled by different colors and signs.

Table 2 lists the details for the global buoys used in this paper. The buoy IDs, missions, longitude and latitude for the tropics and subtropics are shown in columns 2 to 5 and columns 6 to 9, respectively. In the case of tropical buoys, the IDs for missions TAO/TRITON, PIRATA and RAMA are denoted by locations ranging from No. 1 to 57 in the 1st column of tropical buoys, while IDs ranging from No. 58 to 69 are categorized by NDBC. The buoy in the southeastern Indian Ocean is named Bailong, while those in the South China Sea (SCS) are denoted by SF304 and Nansha, respectively (Feng et al., 2020; Liu, Y et al., 2021). For the subtropical buoys, the IDs ranging from No. 1 to 37 in the 5th column of subtropical buoys are categorized by NDBC, while the PMEL buoys in the north Pacific are named KEO and Papa.

**Table 2.** List of Buoy Information Used in this Study.

| | Tropical | | | | Subtropical | | | |
|---|---|---|---|---|---|---|---|---|
| | ID | Mission | Lon (°) | Lat (°) | ID | Mission | Lon (°) | Lat (°) |
| 1 | 0n95w | TAO/TRITON | -95.0 | 0.0 | 41001 | NDBC | -72.3 | 34.7 |
| 2 | 0n110w | TAO/TRITON | -110.0 | 0.0 | 41002 | NDBC | -75.0 | 32.0 |
| 3 | 0n125w | TAO/TRITON | -125.0 | 0.0 | 41010 | NDBC | -78.5 | 28.9 |
| 4 | 0n140w | TAO/TRITON | -140.0 | 0.0 | 41046 | NDBC | -68.4 | 23.8 |
| 5 | 0n156e | TAO/TRITON | 156.0 | 0.0 | 41047 | NDBC | -71.5 | 27.5 |
| 6 | 0n165e | TAO/TRITON | 165.0 | 0.0 | 41048 | NDBC | -69.6 | 31.8 |
| 7 | 0n180w | TAO/TRITON | -180.0 | 0.0 | 41049 | NDBC | -62.9 | 27.5 |
| 8 | 2n95w | TAO/TRITON | -95.0 | 2.0 | 42001 | NDBC | -89.7 | 25.9 |
| 9 | 2n125w | TAO/TRITON | -125.0 | 2.0 | 42002 | NDBC | -93.7 | 26.1 |
| 10 | 2n140w | TAO/TRITON | -140.0 | 2.0 | 42003 | NDBC | -85.6 | 25.9 |
| 11 | 2n165e | TAO/TRITON | 165.0 | 2.0 | 42022 | NDBC | -83.7 | 27.5 |
| 12 | 2n170w | TAO/TRITON | -170.0 | 2.0 | 42023 | NDBC | -83.1 | 26.0 |
| 13 | 2n180w | TAO/TRITON | -180.0 | 2.0 | 42026 | NDBC | -83.5 | 25.2 |
| 14 | 2s95w | TAO/TRITON | -95.0 | -2.0 | 42047 | NDBC | -93.6 | 27.9 |
| 15 | 2s110w | TAO/TRITON | -110.0 | -2.0 | 42360 | NDBC | -90.5 | 26.7 |
| 16 | 2s140w | TAO/TRITON | -140.0 | -2.0 | 42395 | NDBC | -90.8 | 26.4 |
| 17 | 2s165e | TAO/TRITON | 165.0 | -2.0 | 44008 | NDBC | -69.3 | 40.5 |
| 18 | 2s170w | TAO/TRITON | -170.0 | -2.0 | 44011 | NDBC | -66.6 | 41.1 |
| 19 | 5n95w | TAO/TRITON | -95.0 | 5.0 | 44066 | NDBC | -72.6 | 39.6 |
| 20 | 5n110w | TAO/TRITON | -110.0 | 5.0 | 46001 | NDBC | -148.0 | 56.2 |
| 21 | 5n125w | TAO/TRITON | -125.0 | 5.0 | 46002 | NDBC | -130.5 | 42.6 |
| 22 | 5n140w | TAO/TRITON | -140.0 | 5.0 | 46006 | NDBC | -137.4 | 40.8 |
| 23 | 5n165e | TAO/TRITON | 165.0 | 5.0 | 46035 | NDBC | -177.7 | 57.0 |
| 24 | 5s110w | TAO/TRITON | -110.0 | -5.0 | 46047 | NDBC | -119.5 | 32.4 |
| 25 | 5s125w | TAO/TRITON | -125.0 | -5.0 | 46059 | NDBC | -130.0 | 38.1 |
| 26 | 5s140w | TAO/TRITON | -140.0 | -5.0 | 46066 | NDBC | -155.0 | 52.8 |
| 27 | 5s155w | TAO/TRITON | -155.0 | -5.0 | 46070 | NDBC | 175.2 | 55.0 |
| 28 | 8n110w | TAO/TRITON | -110.0 | 8.0 | 46072 | NDBC | -172.1 | 51.7 |

| | | | | | | | | |
|---|---|---|---|---|---|---|---|---|
| 29 | 8n125w | TAO/TRITON | -125.0 | 8.0 | 46073 | NDBC | -172.0 | 55.0 |
| 30 | 8n137e | TAO/TRITON | 137.0 | 8.0 | 46075 | NDBC | -160.8 | 54.0 |
| 31 | 8n165e | TAO/TRITON | 165.0 | 8.0 | 46078 | NDBC | -152.6 | 55.6 |
| 32 | 8n170w | TAO/TRITON | -170.0 | 8.0 | 46080 | NDBC | -150.0 | 58.0 |
| 33 | 8s95w | TAO/TRITON | -95.0 | -8.0 | 46085 | NDBC | -142.9 | 55.9 |
| 34 | 8s110w | TAO/TRITON | -110.0 | -8.0 | 46089 | NDBC | -125.8 | 45.9 |
| 35 | 8s125w | TAO/TRITON | -125.0 | -8.0 | 51000 | NDBC | -153.8 | 23.5 |
| 36 | 8s155w | TAO/TRITON | -155.0 | -8.0 | 51001 | NDBC | -162.0 | 24.5 |
| 37 | 0n35w | PIRATA | -35.0 | 0.0 | 51101 | NDBC | -162.1 | 24.4 |
| 38 | 4n23w | PIRATA | -23.0 | 4.0 | KEO | PMEL | 144.6 | 32.3 |
| 39 | 4n38w | PIRATA | -38.0 | 4.0 | Papa | PMEL | -144.9 | 50.1 |
| 40 | 10s10w | PIRATA | -10.0 | -10.0 | | | | |
| 41 | 12n23w | PIRATA | -23.0 | 12.0 | | | | |
| 42 | 15n38w | PIRATA | -38.0 | 15.0 | | | | |
| 43 | 20n38w | PIRATA | -38.0 | 20.0 | | | | |
| 44 | 21n23w | PIRATA | -23.0 | 21.0 | | | | |
| 45 | 0n80.5e | RAMA | 80.5 | 0.0 | | | | |
| 46 | 1.5s80.5e | RAMA | 80.5 | -1.5 | | | | |
| 47 | 4s67e | RAMA | 67.0 | -4.0 | | | | |
| 48 | 4s80.5e | RAMA | 80.5 | -4.0 | | | | |
| 49 | 5s95e | RAMA | 95.0 | -5.0 | | | | |
| 50 | 8n67e | RAMA | 67.0 | 8.0 | | | | |
| 51 | 8s67e | RAMA | 67.0 | -8.0 | | | | |
| 52 | 8s80.5e | RAMA | 80.5 | -8.0 | | | | |
| 53 | 8s95e | RAMA | 95.0 | -8.0 | | | | |
| 54 | 12n90e | RAMA | 90.0 | 12.0 | | | | |
| 55 | 12s67e | RAMA | 67.0 | -12.0 | | | | |
| 56 | 12s80.5e | RAMA | 80.5 | -12.0 | | | | |
| 57 | 15n90e | RAMA | 90.0 | 15.0 | | | | |
| 58 | 41040 | NDBC | -53.1 | 14.6 | | | | |
| 59 | 41041 | NDBC | -46.1 | 14.3 | | | | |

| | | | | |
|---|---|---|---|---|
| 60 | 41043 | NDBC | -64.8 | 21.0 |
| 61 | 41044 | NDBC | -58.6 | 21.6 |
| 62 | 42055 | NDBC | -93.9 | 22.1 |
| 63 | 42056 | NDBC | -85.0 | 19.8 |
| 64 | 42057 | NDBC | -81.4 | 16.9 |
| 65 | 42058 | NDBC | -74.6 | 14.8 |
| 66 | 42059 | NDBC | -67.5 | 15.3 |
| 67 | 42060 | NDBC | -63.3 | 16.4 |
| 68 | 51002 | NDBC | -157.7 | 17.0 |
| 69 | 51004 | NDBC | -152.3 | 17.5 |
| 70 | SF304 | MNR | 115.5 | 19.9 |
| 71 | Bailong | MNR | 115.2 | -16.9 |
| 72 | Nansha | MNR | 115.6 | 9.95 |

*Note*. Positive (negative) longitude represents east (west) longitude, and positive (negative) latitude represents north (south) latitude. The IDs of TAO/TRITON, PIRATA and RAMA have a number and letter combination for latitude in the first half and a number and letter combination for longitude in the second half. For example, the buoy located at 0°N and 95°W is named ‘0n95w’. The NDBC IDs are named by the five numbers assigned by the World Meteorological Organization (WMO). The first two numbers represent large areas where the buoys are located (41-the Atlantic off of the southeast U.S. coast, 42-the Gulf of Mexico, 44-the Atlantic Ocean north of North Carolina, 46-the U.S. coastal Pacific Ocean, and 51-the Hawaii Islands), while the last three numbers represent specific buoy locations (NDBC, https://www.ndbc.noaa.gov/staid.shtml).

### 2.2 Methods

The CSCAT Level 2 data affected by land, rainfall and sea ice were excluded through quality flags in the system. For the buoy data, the high-frequency wind parameters (e.g., the wind direction and speed) of measurements are normally averaged and recorded over a specified temporal interval. The singular values of observations were eliminated by means of manual inspection in two steps: first, physically reasonable air-sea variables observed by the buoys were judged in a specified range (e.g., 0 to 30 $ms^{-1}$ for wind speed and 0 to 30°C for sea surface temperature, SST); second, the removed singular values were obtained again using a linear interpolation based on the nearest samples. The temporal and spatial differences (collocation) between CSCAT and buoys were limited to no more than 30 min and 25 km, respectively (Gilhousen, 1987; Dickinson et al., 2001). For example, when CSCAT scanned the sea surface wind at a specified time/grid, the program searches the nearby buoy observations within 25 km in space and 30 min in time. Thus, the comparison in this study cannot avoid the inevitable uncertainties resulting from the space and time parameters. For example, in the maritime continent region where extensive high-frequency air-sea-land processes are significant, the differences might be higher. In general, a flow chart of the data verification process is shown in Figure 2.

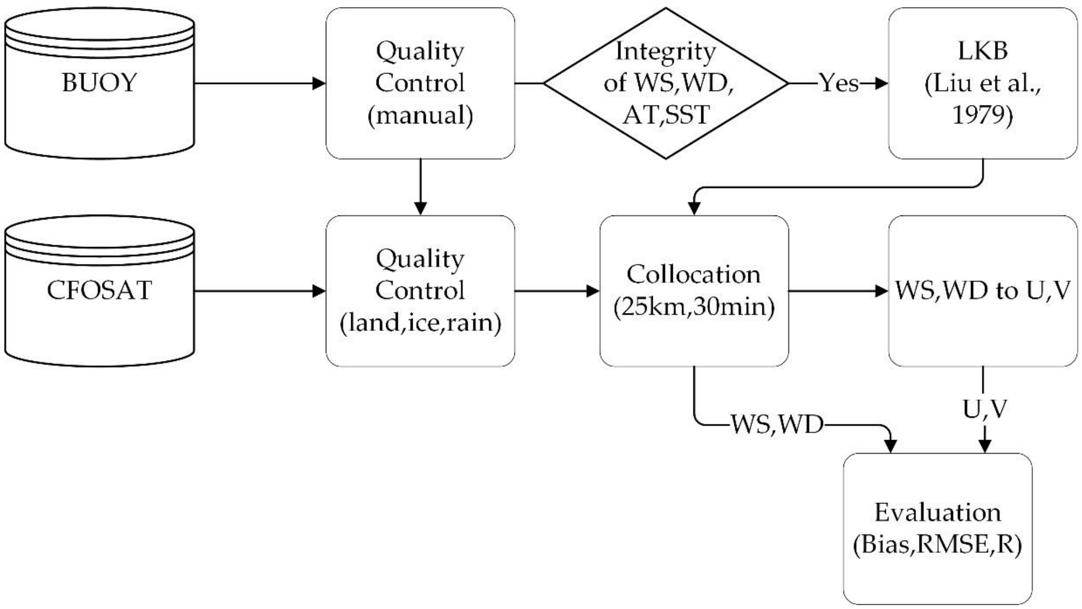


**Figure 2.** Flow chart of CFOSAT evaluation with respect to buoys. WS, WD, AT, SST, U, and V represent wind speed, wind direction, near-surface air temperature, sea surface temperature, zonal wind, and meridional wind, respectively.

The reference height of the sea surface winds observed by the satellite is 10 m above the sea surface. The buoy wind speeds at various heights were converted to equivalent neutral winds at a height of 10 m using the Liu-Katsaros-Businger (LKB) model, and the formulas are as follows (Liu, W T et al., 1979; Jourdan & Gautier, 1995; Liu, W T & Tang, 1996):

$$(T - T_s)/T_* = 2.2\left[\ln(z/z_T) - \psi_T\right] \qquad (1)$$

$$(Q - Q_s)/Q_* = 2.2\left[\ln(z/z_Q) - \psi_Q\right] \qquad (2)$$

$$(U - U_s)/U_* = 2.5\left[\ln(z/z_0) - \psi_U\right] \qquad (3)$$

where U, T, and Q are the wind speed, air temperature, and specific humidity at a height of z. The subscript s indicates that the value of the attached variable is evaluated at the surface. $U_*$, $T_*$, and $Q_*$ are the friction velocity, temperature scale, and humidity scale, which are defined as functions of wind stress, sensible heat flux, and latent heat flux. $\psi_U$, $\psi_T$, and $\psi_Q$ are functions of the stability parameter z/L, where L is the Monin-Obukhov length. $z_T$, $z_Q$ and $z_0$ are the roughness lengths for velocity, temperature, and humidity, respectively. When U, T, Q and their corresponding heights, as well as $T_S$ (SST), are known, it is assumed that $U_S$ is 0, $Q_S$ is the saturation humidity calculated by $T_S$, and three flux values can be solved according to the three implicit equations.

The parameters required by the LKB model are wind speed, air temperature, SST, specific humidity, air pressure and their observation heights. Specific humidity can also be calculated from dew point air temperature (DPAT) or relative humidity (RH). However, compared with the optional air pressure and specific humidity, air temperature and SST are more important parameters in the LKB model. Thus, buoys with simultaneous wind speed, wind direction, SST, and air temperature were chosen in this paper. The available time series for each buoy is shown in Figure 2. The number of effective observations that can be used for comparisons in tropical oceans is higher than that in subtropical oceans.

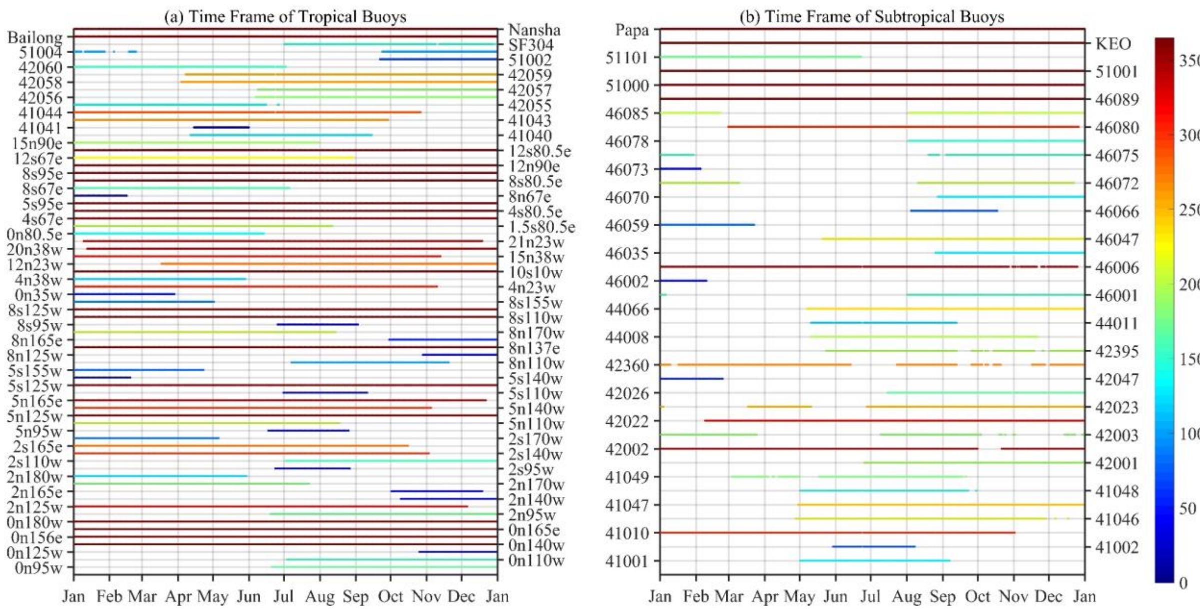


**Figure 3.** Time frame of buoy observations in 2019 used in this study. (a) Time frame of tropical buoys. (b) Time frame of subtropical buoys. Note that the actual time frame of some buoys may be longer than listed here. The available time frame represents the period for which the wind speed, wind direction, SST, and near-surface air temperature are available from the buoy so that wind speed can be converted to neutral wind at 10 m. The color bar indicates the duration (number of days) of observations available for each buoy.

The accuracy of CSCAT wind speed, wind direction, meridional wind, and zonal wind were tested. The error statistics of the test were selected as the mean bias error (Bias, Eq. (4)), root-mean-square error (RMSE, Eq. (5)) and the Pearson correlation coefficient (R, Eq. (6)).

$$Bias = \sum_{i=1}^{n} (w_i^c - w_i^b) \Big/ n \qquad (4)$$

$$RMSE = \sqrt{\sum_{i=1}^{n} (w_i^c - w_i^b)^2 \Big/ n} \qquad (5)$$

$$R=\frac{\sum_{i=1}^{n}\left(w_i^c-\overline{w_i^c}\right)\left(w_i^b-\overline{w_i^b}\right)}{\sqrt{\sum_{i=1}^{n}(w_i^c-w_i^c)^2\sum_{i=1}^{n}(w_i^b-w_i^b)^2}} \qquad (6)$$

where n is the number of collocated samples, $w^b$ is the wind speed, direction, zonal, and meridional wind observed by the buoy and $w^c$ represents the CFOSAT observations.

## 3 Validation of CSCAT winds compared to the buoy observations

### 3.1 Collocated samples in CSCAT and buoys

The valid wind speed range of CSCAT observations is 4-24 $ms^{-1}$, while wind speeds below 4 $ms^{-1}$ are beyond the designed measurement range, which is an important part of the global wind distribution, for example, in the region of the tropics. The collocated CSCAT winds and buoy measurements from 4 $ms^{-1}$ to 24 $ms^{-1}$ and 0 $ms^{-1}$ to 4 $ms^{-1}$ in the tropics and subtropics were compared, respectively. Wind speeds cannot be negative, and the error cannot vary normally with the wind speeds, especially when the wind speeds are close to 0 $ms^{-1}$, which leads to a more positive bias at low wind speeds and skews the overall mean bias (Freilich, 1997; Dickinson et al., 2001). Therefore, in addition to wind speed and wind direction, zonal wind and meridional wind were also examined in this study.

In total, 13724 pairs of collocated CSCAT and buoy data were found in the range of 4-24 $ms^{-1}$, while 2718 pairs were found in the 0-4 $ms^{-1}$ range (Figure 4). The collocated data were counted in each month, as shown in Figure 3. The proportion of wind speeds in the range of 0-4 $ms^{-1}$ was lower than 13.9% in winter, which was significantly lower than the minimum value of 16.0% in other months. The reason may be that most of the buoys are located in the Northern Hemisphere, and the wind speeds in winter are higher than those in other seasons, resulting in a lower proportion in the range of 0-4 $ms^{-1}$. However, due to a scatterometer anomaly occurring on 20 December 2019, the missing data accounted for approximately one-third of the total samples in December.

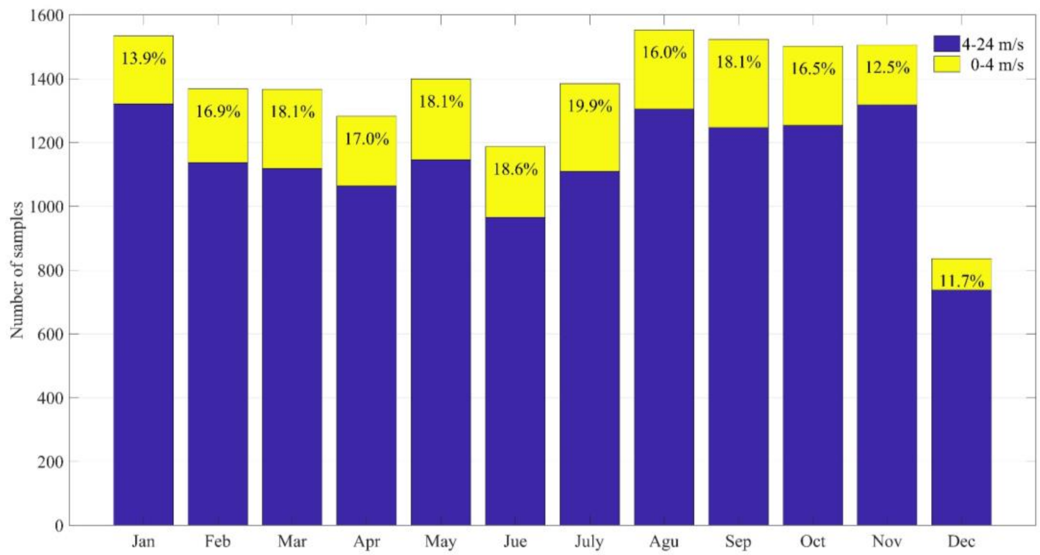


**Figure 4.** Number of samples in each month of 2019. The blue bars represent the number of samples in the wind range of 4-24 $ms^{-1}$, while the yellow bars denote the number of samples in the wind range of 0-4 $ms^{-1}$. The numbers inside the yellow bars represent the ratios of the samples for each month in the wind speed range of 0-4 $ms^{-1}$.

### 3.2 Evaluation of wind speed, wind direction, zonal wind, and meridional wind

Before evaluation, CSCAT winds were collocated with global buoy observations. Figure 5 shows that the CSCAT winds agree well with those for global buoys in the range of 4-24 $ms^{-1}$. The bias, RMSE, and R are -0.1 $ms^{-1}$, 1.1 $ms^{-1}$ and 0.91 for wind speed, respectively, which are much lower than the designed RMSE requirement of 2 $ms^{-1}$. For the wind direction, the bias, RMSE and R are 1.4°, 20.4° and 0.98, respectively, which are slightly higher than the RMSE requirement of 20°. The bias, RMSE and R are 0.1 $ms^{-1}$, 1.6 $ms^{-1}$ and 0.96 for the zonal wind and 0.1 $ms^{-1}$, 1.7 $ms^{-1}$ and 0.94 for the meridional wind, respectively. The validation results for zonal wind are slightly better than those of meridional wind.

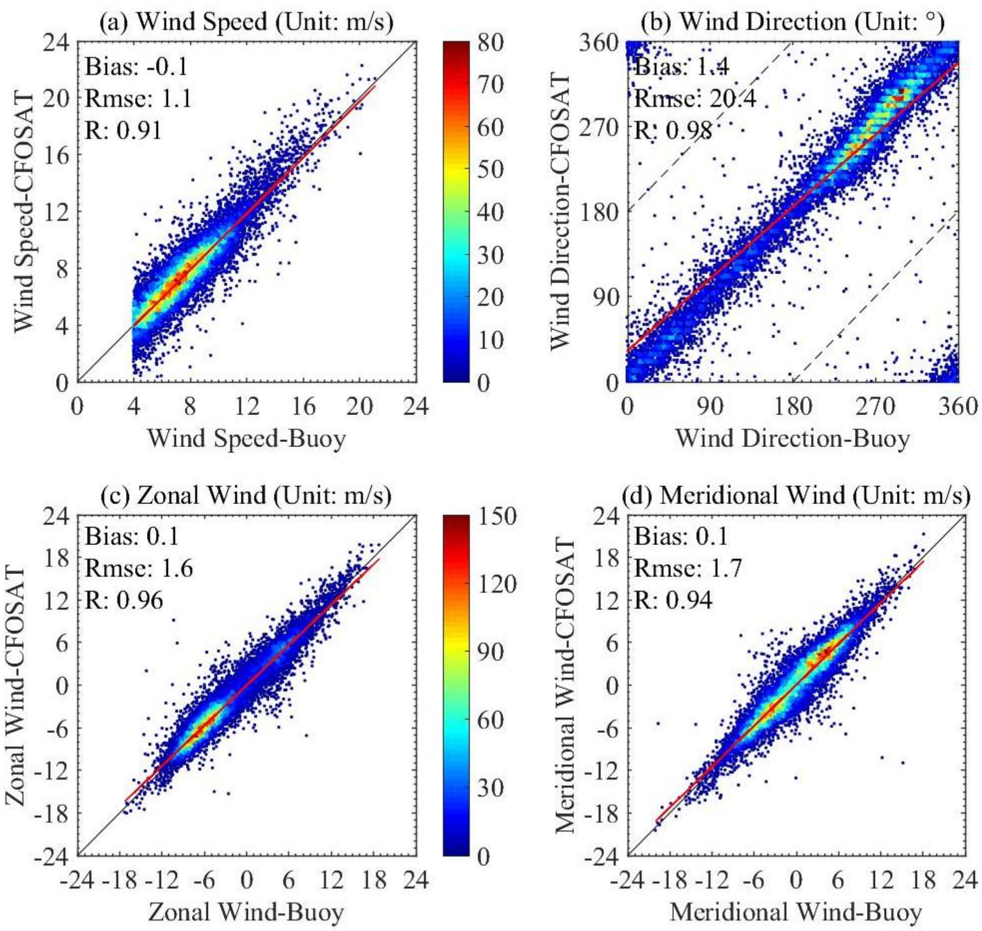


**Figure 5.** Scatterplots of the (a) wind speed (unit: $ms^{-1}$), (b) wind direction (unit: °), (c) zonal wind (unit: $ms^{-1}$), and (d) meridional wind (unit: $ms^{-1}$) between CFOSAT and global buoys in the range of 4-24 $ms^{-1}$. The x-axis represents the buoy results, while the y-axis represents the CFOSAT results. Colors represent the occurrence in wind speed bins of 0.24 ms-1×0.24 $ms^{-1}$, wind direction bins of 3.6°×3.6°, zonal wind bins of 0.48 $ms^{-1}$×0.48 $ms^{-1}$ and meridional wind bins of 0.48 $ms^{-1}$×0.48 $ms^{-1}$.

CSCAT observations in the range of 0-4 $ms^{-1}$ are not the main focus of this study; however, they have similar performance. As shown in Figure 6, the performance of global CSCAT data below 4 $ms^{-1}$ is poorer than that of wind speeds ranging from 4 to 24 $ms^{-1}$. The bias, RMSE and R are 0.3 $ms^{-1}$, 1.3 $ms^{-1}$ and 0.46 for wind speed; -0.8°, 62.6° and 0.83 for wind direction; -0.1 $ms^{-1}$, 1.8 $ms^{-1}$ and 0.65 for zonal wind; and −0.1 $ms^{-1}$, 1.9 $ms^{-1}$ and 0.62 for meridional wind, respectively. The scatterplot shows poorer fits for the wind speed, wind direction and wind components than those in the range of 4-24 $ms^{-1}$. A larger bias and RMSE and a lower R are observed when the wind speeds are distributed in the range of 0-4 $ms^{-1}$, which is mainly due to the buoy's delayed response to low winds and the absence of Bragg waves at low wind speeds (Donelan & Pierson, 1987). The similarity between the two wind speed ranges is that the zonal wind is slightly better than the meridional wind, which may be due to the higher wind speeds of the zonal wind. Wind speeds below 4 $ms^{-1}$ in the tropics and subtropics showed results similar to those at the global scale, which are not shown here to avoid repetition.

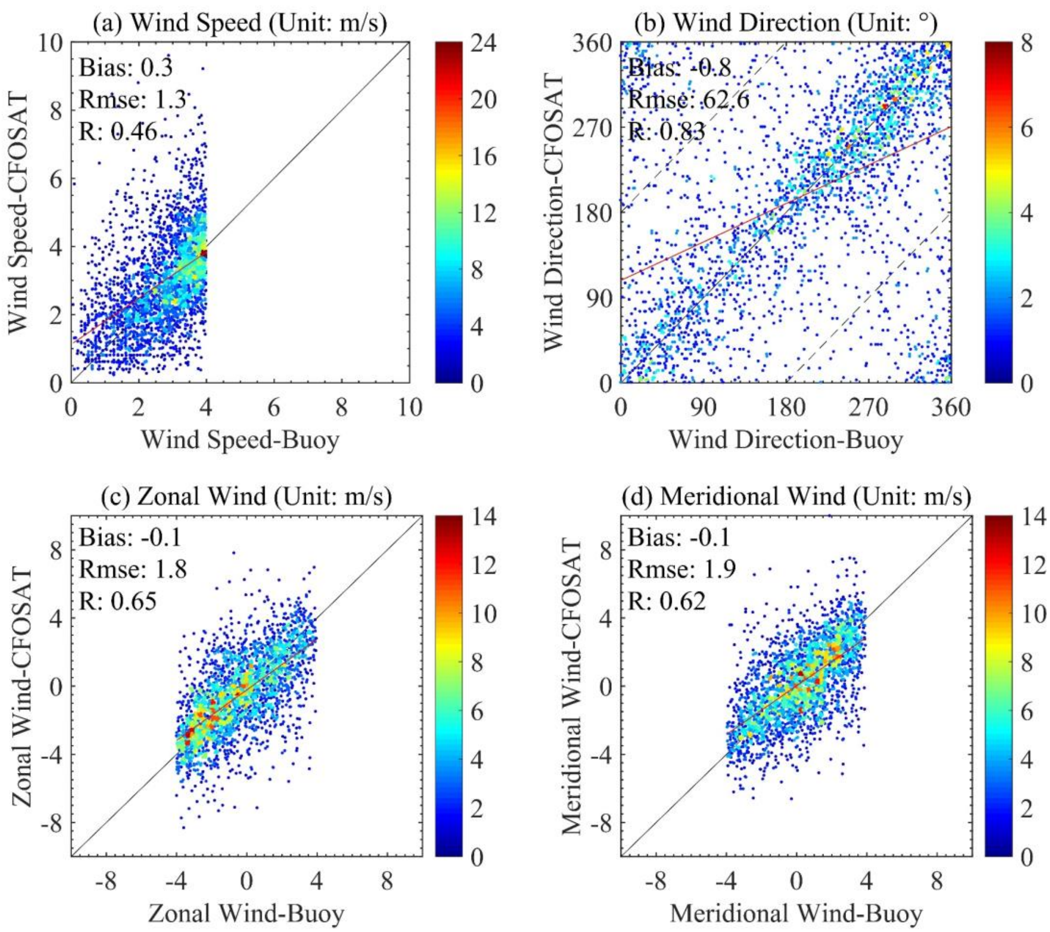


**Figure 6.** The same as in Figure 5 but for wind speeds in the range of 0-4 $ms^{-1}$.

Figure 7 shows that the RMSE of CSCAT wind in the tropics is larger than that at the global scale, and bias and R exhibit similar results. The bias and RMSE increase to -0.1 $ms^{-1}$ and 1.1 $ms^{-1}$ for the wind speed, 1.2° and 21.5° for the wind direction, 0.1 $ms^{-1}$ and 1.5 $ms^{-1}$ for the zonal wind, and 0.1 $ms^{-1}$ and 1.7 $ms^{-1}$ for the meridional wind, while the corresponding R values decrease to 0.86, 0.96, 0.94 and 0.92, respectively. Possible reasons for the lower accuracy in the tropics are that the wind speeds are generally lower than those in the subtropics and that the influence of sea surface currents is larger. The results are consistent with previous studies, which found that the influence of surface currents on wind estimates is greatest in the tropics (Luo et al., 2005; Dawe & Thompson, 2006; Brodeau et al., 2016). The scatters have a good linear distribution in Figure 8. Comparisons show that the R of wind speeds reaches 0.94, and CSCAT observations agree well with the buoy observations in the subtropics (Figure 8a). The winds collocated in the subtropics achieve lower bias, lower RMSE and higher R than the global and tropical winds. The RMSEs of wind speed, wind direction, zonal wind, and meridional wind decrease to 1.1 $ms^{-1}$, 18.8°, 1.7 $ms^{-1}$ and 1.7 $ms^{-1}$, respectively, which meet the accuracy requirements of 2 $ms^{-1}$ and 20° for wind speed and wind direction. The corresponding Rs values increase to 0.94, 0.98, 0.97 and 0.96.

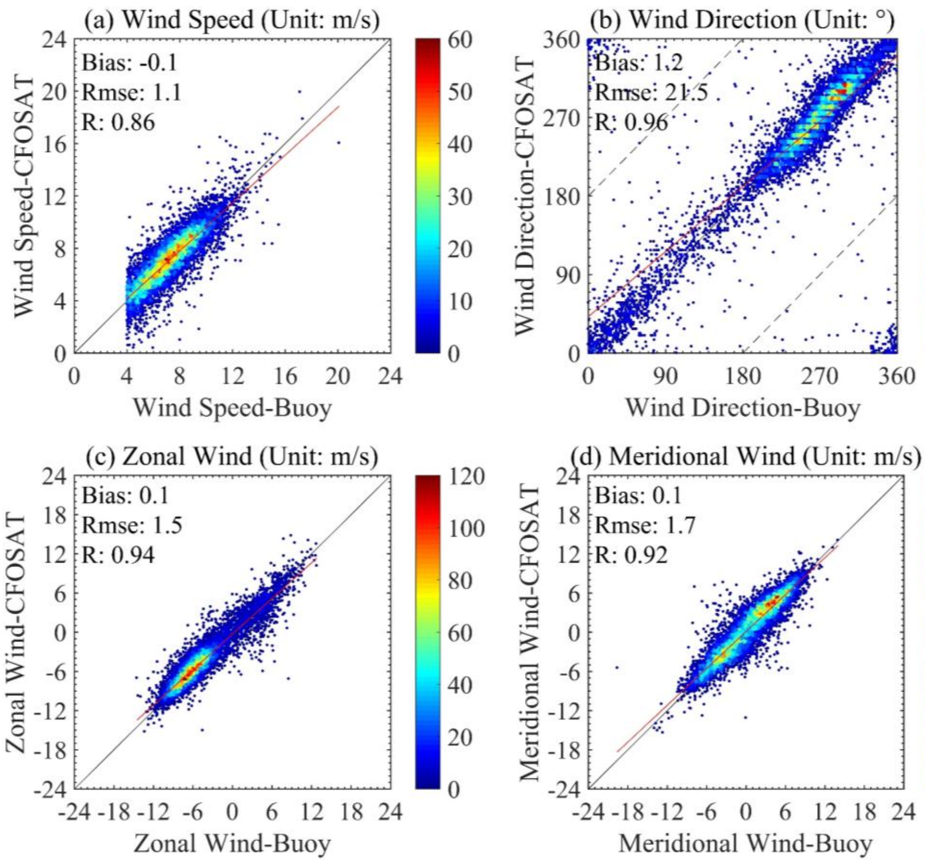


**Figure 7.** The same as in Figure 5 but for the tropics based on the buoys listed on the left of Table 2.

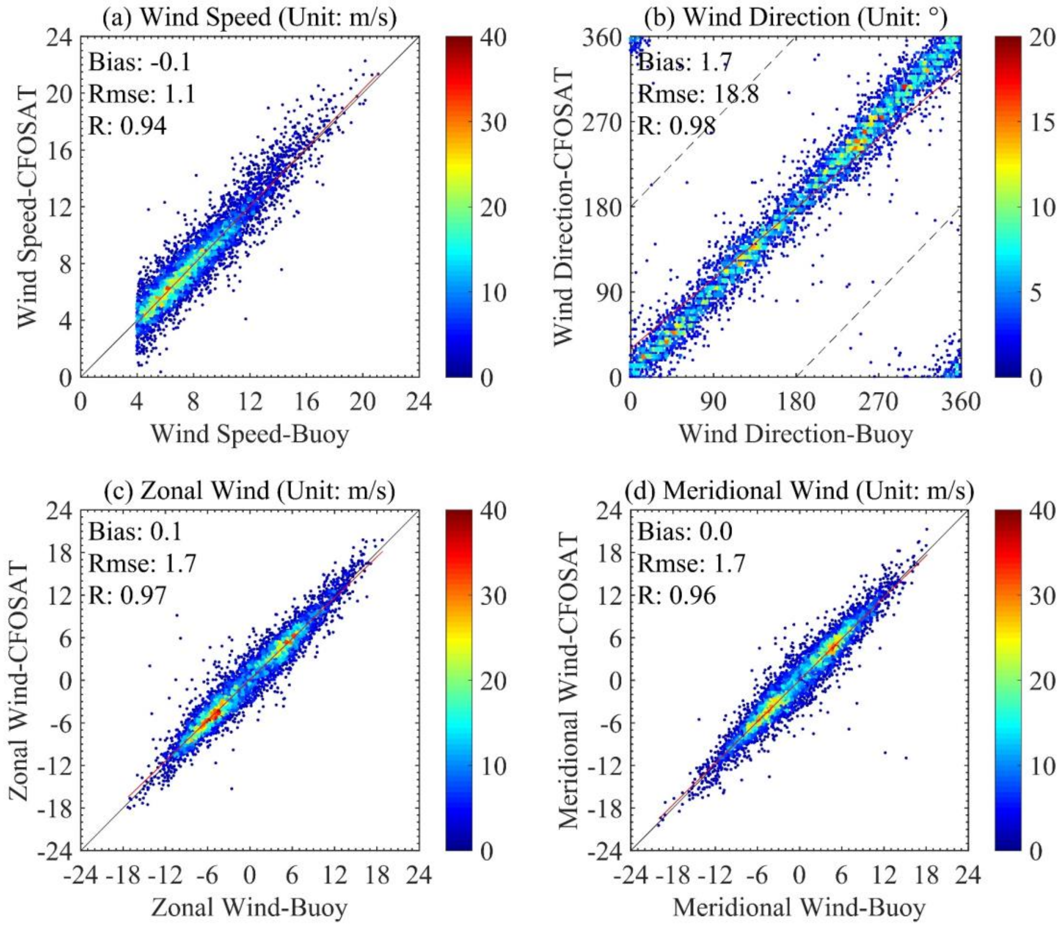


**Figure 8.** The same as in Figure 5 but for the subtropics based on the buoys listed on the right of Table 2.

The comparison of wind directions observed by collocated CSCAT and buoys in Figure 9 shows that the east wind clearly accounts for a large proportion. The rose diagram is divided into five wind speed ranges, namely, 0-4 $ms^{-1}$, 4-6 $ms^{-1}$, 6-8 $ms^{-1}$, 8-10 $ms^{-1}$ and above 10 $ms^{-1}$. Three major characters can be found in Figure 9. First, easterly winds are dominant in terms of the rose plots because there are more tropical buoy observations than subtropical observations (Figure 2). Second, CSCAT indicates good-quality wind observations compared with the *in situ* buoy observations, and the CSCAT high winds ranging from 8 to more than 10 $ms^{-1}$ agree better with the buoy observations than those below 6 $ms^{-1}$. Third, the number of buoy observations below 6 $ms^{-1}$ is slightly larger than that of CSCAT, and the number of CSCAT winds above 6 $ms^{-1}$ is slightly larger than that of the buoys. Although wind speeds below 4 $ms^{-1}$ are beyond the designed technical aim of CSCAT, fairly good agreement with the buoy observations is obtained.

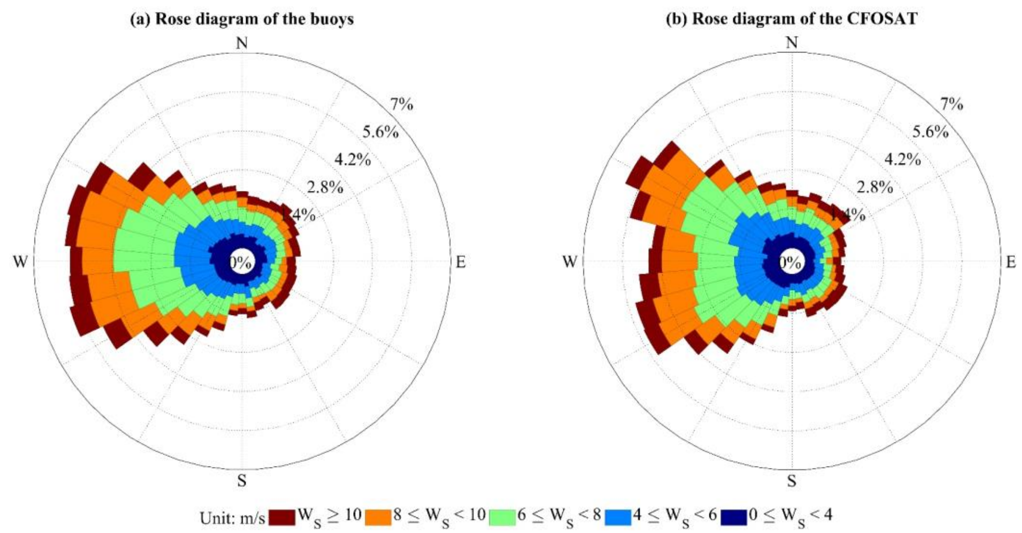


**Figure 9.** Rose diagrams of collocated buoy and CSCAT in 2019. (a) Rose diagram of buoy measurements; (b) Rose diagram of CSCAT observations.

Figure 10 displays the RMSEs of CSCAT wind speed, wind direction, zonal wind, and meridional wind with respect to the global buoys, which indicates that the southern Indian Ocean, the western Pacific warm pool (WPWP) and areas close to land are subject to higher potential impacts. Combining the wind speed, wind direction, zonal wind, and meridional wind, the satellite observations indicate fairly good quality in the ocean interior and the Gulf of Mexico and Gulf Stream. In terms of global wind speed, there are only two buoys with RMSEs close to 2 $ms^{-1}$. There are 37 buoys with RMSEs of wind direction greater than 20°, of which 12 are in the subtropics and 25 are in the tropics. The maximum RMSE in the wind direction between the satellite and buoy observations can reach 50°. In particular, the wind direction errors of the buoys located at 165°E are relatively large, which may be caused by complex local sea-air-land interactions (Figure 10b). Thus, special attention should be paid to the wind direction when using the CSCAT data in the WPWP. A similar structure in wind direction can also be found in the eastern tropical Indian Ocean, which is a part of the Indo-Pacific warm pool. In the maritime continental region, extensive air-sea-land processes are significant, which affects the accuracy of CSCAT with relatively low temporal resolution.

In terms of the Rs between CSCAT and global buoy observations, the Rs in the subtropical region is significantly higher than that in the tropical region (Figure 11). The regions with lower Rs are mainly in the tropical Pacific, which may be due to the relatively high ocean current velocity and relatively low wind speeds. For wind speed, Rs in tropical regions is basically greater than 0.6, while that in subtropical regions is basically above 0.8. In terms of wind direction, Rs in tropical regions is basically greater than 0.6, and Rs in subtropical regions is above 0.9. The Rs of meridional and zonal winds are similar, mostly above 0.6 in the tropics and above 0.9 in the subtropics. Although the RMSEs in the WPWP are larger than those in other regions, the Rs shows good agreement between the satellite and *in situ* buoy observations.

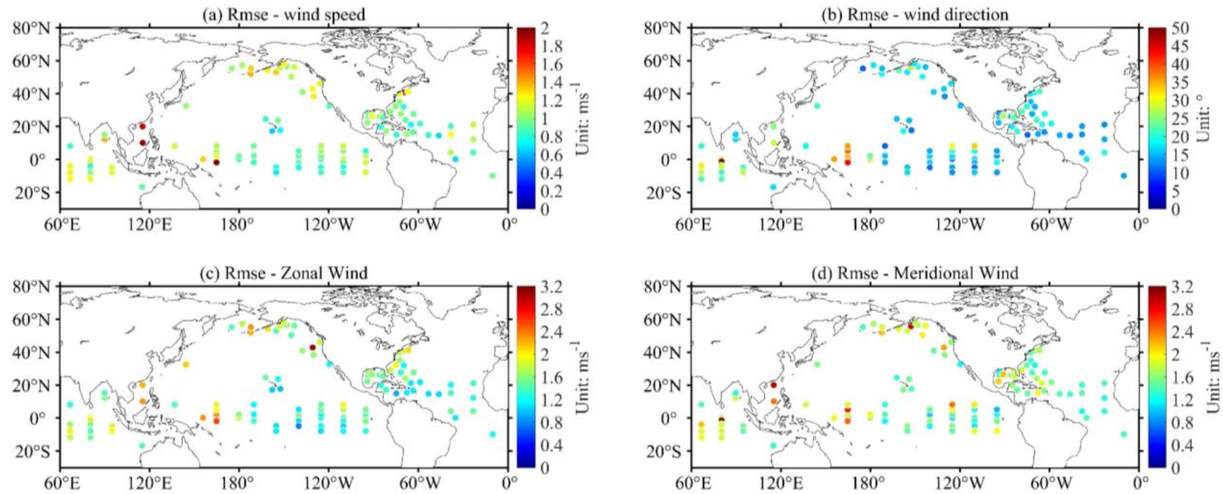


**Figure 10.** RMSEs of the (a) wind speed (unit: $ms^{-1}$), (b) wind direction (unit: °), (c) zonal wind (unit: $ms^{-1}$), and (d) meridional wind (unit: $ms^{-1}$) at each buoy site. Colors represent the RMSE values.

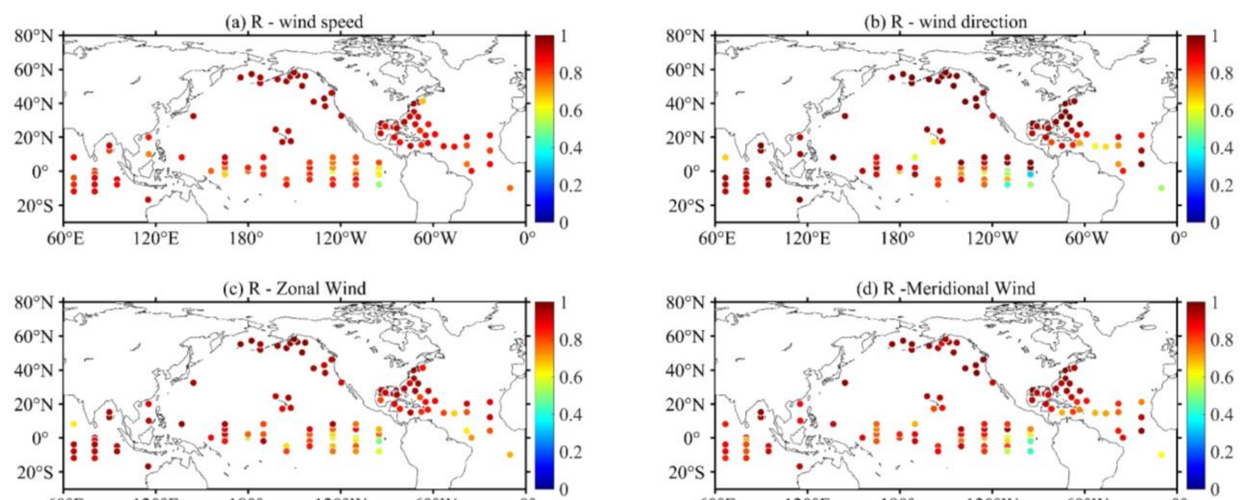


**Figure 11.** The same as in Figure 10 but for the Rs.

Among all buoys over the global oceans, the Chinese observations contribute to the community in terms of the Bailong buoy seated to the northwest of Australia, the SF304 buoy in the north of the SCS, and the Nansha buoy in the south of the SCS. CSCAT performs better in the southeastern Indian Ocean, with lower discrepancies in the wind speed, wind direction, zonal wind, and meridional wind than those in the SCS. The magnitudes of the bias, RMSE, and R in the wind direction are 4.5°, 15.1° and 0.99, respectively, compared to the Bailong buoy, whereas the magnitudes are -13.9°, 25.2° and 0.95, respectively, in the north of the SCS and -1.9°, 28.1° and 0.96, respectively, in the south of the SCS. The magnitudes of the wind speed bias, RMSE and R are -0.2 $ms^{-1}$, 0.9 $ms^{-1}$ and 0.89 for the Bailong buoy, 0.5 $ms^{-1}$, 1.8 $ms^{-1}$ and 0.86 for the SF304 buoy, and 0.3 $ms^{-1}$, 2.0 $ms^{-1}$ and 0.74 for the Nansha buoy, respectively. The results indicate that CSCAT shows a better consistency with the Bailong buoy than those of SF304 and Nansha. Similar results can also be found for the zonal and meridional winds but are not shown here to avoid repetition. However, the Bailong, SF304 and Nansha buoys help us understand the quality of CSCAT in East Asia, where *in situ* observations are sparse.

Ocean currents near the equator bring significant relative errors in wind stress, especially in the South Equatorial Current (SEC), the North Equatorial Countercurrent (NECC) and the North Equatorial Current (NEC) (Brodeau et al., 2016). In this study, the results are consistent with previous studies, except for the region of the NEC where no available buoys were collected. Larger errors are found in the NECC in the Pacific Ocean (Donguy & Meyers, 1996; Yu, Z et al., 2000), the SEC in the Atlantic Ocean (Bonhoure et al., 2004), and the monsoon area in the Indian Ocean (Schott & Mccreary, 2001), where ocean currents are sufficiently strong with respect to wind speeds. In addition, the uncertainty in the wind stress over the western boundary current (WBC) region due to the presence of surface currents has been shown to have significant effects along the WBC system, including the Loop Current, the Florida Current, and the Gulf Stream and its extensions (Song, 2021). The WBC currents have an independent dynamic mechanism and do not have to flow in the same direction as the local surface wind, which may significantly change the relative wind speed (Song, 2021). In the North Pacific, larger errors in the wind parameters can also be found in the eastern boundary currents, which needs to be further explored in future studies. Overall, this study indicates that large errors exist along equatorial current systems and boundary currents, which are greatly affected by surface currents and sea-air-land interactions.

### 3.3 Analysis of the effects of sea surface currents on comparisons

Among the 111 selected buoys, six buoys with current observations at a depth of no more than 16 m were used to diagnose the effects of surface currents on scatterometer observations. The bias, RMSE and R were still chosen as the error statistics to compare the conditions, including and excluding the influence of ocean currents in the range of 4-24 $ms^{-1}$. Previous studies demonstrated the effects of surface currents on wind measurements by scatterometers in the tropics using TAO/TRITON observations since the scatterometer measures the motion of the air relative to the ocean surface (Dickinson et al., 2001; Kelly et al., 2001; Ebuchi et al., 2002).

The values in and out of the parentheses in Table 3 are the results of excluding and not excluding the influence of surface currents, respectively. The CSCAT wind speed, wind direction, zonal wind, and meridional wind results in the tropicals were almost improved by excluding surface currents. The RMSEs of CSCAT wind speeds verified by the four tropical buoys (0n110w, 0n140w, 0n156e, 8n137e) decreased from 1.2 $ms^{-1}$, 0.9 $ms^{-1}$, 1.3 $ms^{-1}$ and 1.1 $ms^{-1}$ to 1.1 $ms^{-1}$, 0.8 $ms^{-1}$, 1.2 $ms^{-1}$ and 1.1 $ms^{-1}$, respectively, while the RMSEs of wind direction decreased from 16.3°, 15.0°, 35.3° and 18.1° to 14.3°, 13.2°, 34.8° and 17.9°, respectively, and the corresponding R values also improved. The results show that the two buoys located in the SEC (0°N, 110°W and 0°N, 140°W) improved more than the other tropical buoys after excluding the surface currents, which may be related to the strong velocity and low wind speed in the equatorial Pacific. For the wind vector component in the tropical region, the RMSEs of CSCAT zonal wind before and after the removal of the currents decreased from 1.6 $ms^{-1}$, 1.2 $ms^{-1}$, 2.3 $ms^{-1}$ and 1.4 $ms^{-1}$ to 1.4 $ms^{-1}$, 0.9 $ms^{-1}$, 2.2 $ms^{-1}$ and 1.4 $ms^{-1}$, respectively, while the RMSEs of meridional wind changed from 1.1 $ms^{-1}$, 1.5 $ms^{-1}$, 1.9 $ms^{-1}$ and 1.8 $ms^{-1}$ to 1.1 $ms^{-1}$, 1.4 $ms^{-1}$, 1.9 $ms^{-1}$ and 1.8 $ms^{-1}$, respectively. The tropical zonal wind obviously improved greatly after removing the current influence, but the meridional changes were small or did not show improvement. One possible reason is that the east-west current in the tropics dominates, while the north-south current is relatively weak. The average ratio of current velocity to wind speed for six buoys was calculated (the last row in Table 3). In the equatorial region (0n110w, 0n140w, and 0n156e), the ratios are larger, which are 0.12, 0.07 and 0.06, respectively, and the corresponding results are greatly improved. The other tropical region (8n137e) has a ratio of 0.03, but the results are still slightly improved. The improvement of wind speed and wind direction is different, which is related to the angle between the surface current direction and wind direction. However, in the subtropics (KEO and Papa), the ratios are lower, 0.04 and 0.02, respectively, and the validation results after removing the influence of ocean currents did not improve. Based on limited ocean current data, this study indicates that in the tropics, surface currents have a great influence on scatterometer observations, while in the subtropics, surface currents are not the main factor affecting scatterometer accuracy. In future studies, with the increase in available data, explorations of the surface current influence on scatterometer observations will continue.

**Table 3.** Comparison of Results Including and Excluding the Surface Surrents. The numbers in parentheses are the results of excluding the surface curents, and the buoy ID represents the buoy location.

| | Measures | 0n110w | 0n140w | 0n156e | 8n137e | KEO(32n145e) | Papa(50n145w) |
|---|---|---|---|---|---|---|---|
| WS ($ms^{-1}$) | Bias | -0.5 (-0.1) | 0.0 (0.1) | -0.5 (-0.3) | 0.1 (0.1) | 0.1 (0.1) | -0.4(-0.4) |
| | RMSE | 1.2 (1.1) | 0.9 (0.8) | 1.3 (1.2) | 1.1 (1.1) | 1.1 (1.1) | 1.1(1.1) |
| | R | 0.72 (0.77) | 0.80 (0.85) | 0.78 (0.79) | 0.86 (0.86) | 0.94(0.95) | 0.96(0.96) |
| WD (°) | Bias | 4.3 (1.1) | 8.7 (7.2) | 1.9 (1.2) | -2.4 (-1.8) | 1.4 (1.4) | 2.9(3.0) |
| | RMSE | 16.3 (14.3) | 15.0 (13.2) | 35.3 (34.8) | 18.1 (17.9) | 23.6(23.8) | 19.4(19.5) |
| | R | 0.52 (0.54) | 0.81 (0.83) | 0.93 (0.93) | 0.98 (0.98) | 0.97(0.97) | 0.99(0.99) |
| U ($ms^{-1}$) | Bias | 0.6 (0.1) | 0.3 (0.1) | -0.6 (-0.5) | 0.1 (0.1) | 0.0 (-0.1) | 0.1 (0.1) |
| | RMSE | 1.6 (1.4) | 1.2 (0.9) | 2.3 (2.2) | 1.4 (1.4) | 2.1 (2.1) | 1.4 (1.4) |
| | R | 0.54 (0.64) | 0.83 (0.87) | 0.87 (0.88) | 0.97 (0.97) | 0.97(0.97) | 0.98(0.97) |
| V ($ms^{-1}$) | Bias | -0.1 (0.0) | 0.9 (0.8) | 0.0 (0.0) | -0.5 (-0.4) | 0.1 (0.1) | 0.1 (0.1) |
| | RMSE | 1.1 (1.1) | 1.5 (1.4) | 1.9 (1.9) | 1.8 (1.8) | 1.9(1.9) | 2.0 (2.0) |
| | R | 0.71 (0.70) | 0.83 (0.84) | 0.88 (0.89) | 0.91(0.91) | 0.96(0.96) | 0.95 (0.96) |
| | Ratio | 0.12 | 0.07 | 0.06 | 0.03 | 0.04 | 0.02 |

The wind speed retrieved from the scatterometer should be lower than that measured by the anemometer when the surface current tends to flow in the same direction as the wind; conversely, the scatterometer wind speed should be higher when the surface current is opposite to the wind direction (Kelly et al., 2001). Figure 12 shows that in the equatorial Pacific Ocean north of 4°N (2°N in winter), the wind direction is mostly opposite to the NECC, and the corresponding bias is positive. Between 4°N and 5°S in the Pacific Ocean, the wind direction is mostly the same as the equatorial current, and the corresponding bias is negative. For the Pacific buoys south of 5°S, the wind direction is mostly opposite to the SECC, and the corresponding bias is positive. The Indian Ocean south of 10°S is dominated by southeasterly trade winds, and the flow direction of the ocean current is basically stable. The SEC crosses the Indian Ocean from east to west. The Indian Ocean north of 10°S is controlled by the monsoon, and currents change with the seasons. Therefore, the direction of ocean currents in the Indian Ocean is mostly consistent with the wind direction, which is mostly shown as a negative bias. The wind direction in the Atlantic Ocean is basically easterly and consistent with the direction of the ocean current, and the bias is mostly negative.

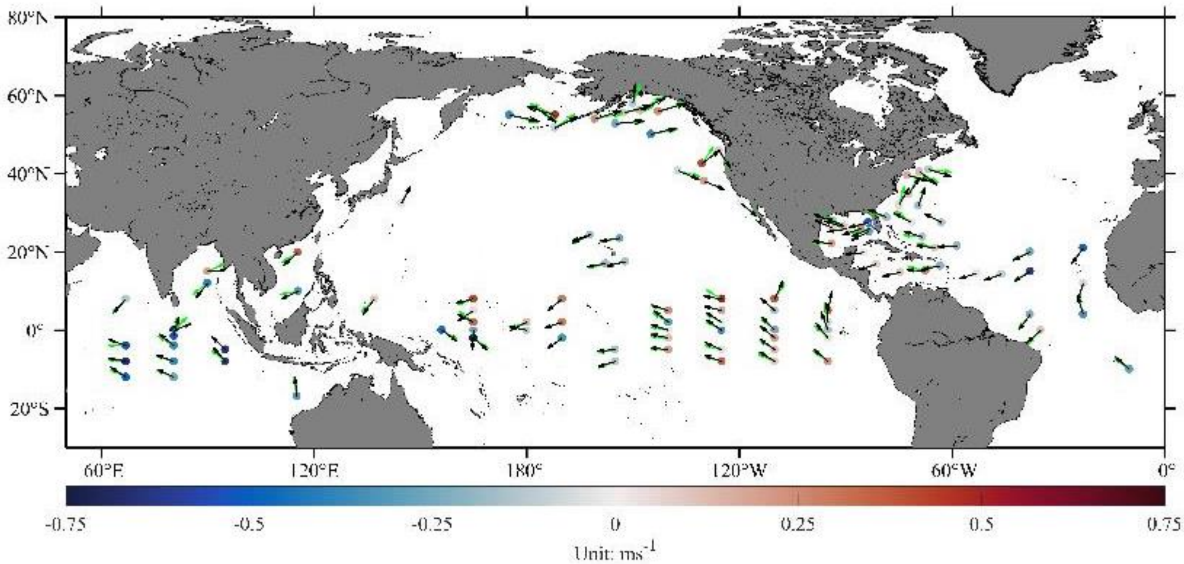


**Figure 12.** The biases in CSCAT wind speeds with respect to global buoys. Colors represent the values of biases (unit: $ms^{-1}$), while the blue arrows and red arrows represent the annual mean wind directions from CSCAT and the buoy at each location, respectively.

## 4 Discussion

The results indicate that the error distribution has evident regional dependence, and the areas with large errors are mainly concentrated in places with strong sea-air-land interactions and high ocean current velocities. The accuracy of scatterometer retrieval depends on different factors, such as location, sea conditions, and other air-sea parameters. Therefore, this study divides the study area into tropical and subtropical regions for future user references.

In the subtropics, the CSCAT wind speeds agree well with the buoy values, and the RMSE of wind direction is 18.8°, meeting the CFOSAT accuracy requirement. However, the RMSE of wind direction is slightly higher than 20° in the tropics, which is close to the accuracy requirement. The validation results in the subtropical regions are better than those in the tropical regions in terms of wind speed, wind direction, zonal wind, and meridional wind. There are several possible explanations. First, the wind speed in the tropics is lower, which might be beyond the designed accuracy of CSCAT. Second, equatorial current systems play a significant role in modifying the relative wind speed between the ocean and atmosphere and thus contribute to larger errors in the tropics (Brodeau et al., 2016). Third, in tropical regions, especially in maritime continental regions, as extensive air-sea-land interactive processes are active, the choice of the collocation method (see Section 2) also results in inevitable errors for CSCAT. Six buoys were used to calculate the influence of surface currents on the scatterometer observations.

According to the validation results from global buoys, both positive and negative biases agree well with the relationship between the current direction and wind direction, which is consistent with the results of previous studies (Ebuchi, 1999; Yu, L & Jin, 2012). Although scatterometer observations have generally improved in the tropics, the zonal wind is greatly affected by the east-west direction of the equatorial current.

**Table 4.** Wind speed (unit: $ms^{-1}$), wind direction (unit: °), zonal wind (unit: $ms^{-1}$), and meridional wind (unit: $ms^{-1}$) error statistics

| | | Global | | | Tropical | | | Subtropical | | |
|---|---|---|---|---|---|---|---|---|---|---|
| | | Bias | RMSE | R | Bias | RMSE | R | Bias | RMSE | R |
| 0-4 $ms^{-1}$ | WS ($ms^{-1}$) | 0.3 | 1.3 | 0.46 | 0.3 | 1.3 | 0.48 | 0.2 | 1.4 | 0.43 |
| | WD (°) | -0.8 | 62.6 | 0.83 | −2.7 | 68.3 | 0.79 | 1.7 | 53.89 | 0.89 |
| | U ($ms^{-1}$) | −0.1 | 1.8 | 0.65 | −0.2 | 1.9 | 0.60 | 0.0 | 1.7 | 0.70 |
| | V ($ms^{-1}$) | −0.1 | 1.9 | 0.62 | −0.1 | 2.0 | 0.55 | 0.0 | 1.7 | 0.71 |
| 4-24 $ms^{-1}$ | WS ($ms^{-1}$) | −0.1 | 1.1 | 0.91 | −0.1 | 1.1 | 0.86 | −0.1 | 1.1 | 0.94 |
| | WD (°) | 1.4 | 20.4 | 0.98 | 1.2 | 21.5 | 0.96 | 1.7 | 18.8 | 0.98 |
| | U ($ms^{-1}$) | 0.1 | 1.6 | 0.96 | 0.1 | 1.5 | 0.94 | 0.1 | 1.7 | 0.97 |
| | V ($ms^{-1}$) | 0.1 | 1.7 | 0.94 | 0.1 | 1.7 | 0.92 | 0.0 | 1.7 | 0.96 |

Moreover, the zonal wind has better error statistics than the meridional wind, which may occur because the sea surface wind is mainly east-west on a global scale (Figure 12) and the zonal wind speed is higher than the meridional wind speed (Figure 5). The low wind speed is one of the reasons that contributes to a large RMSE, and better results may be achieved as the wind speed increases. Low winds are not sufficient to overcome viscous damping, so Bragg waves cannot grow (Donelan & Pierson, 1987). Although as many buoys as possible have been selected in this paper, the areal coverage is still limited, and there is a lack of *in situ* observations, such as buoys at high latitudes in the Northern Hemisphere and in the whole Southern Hemisphere. In addition, coastal performance needs further evaluation. As satellite data accumulate, longer-term evaluations will be carried out, and reanalysis data such as the fifth-generation reanalysis of global climate and atmospheric data provided by the European Centre for Medium-Range Weather Forecasts (ERA5) will be used to conduct a broader global test of CSCAT.

## 5 Conclusions

This study presents a quality assessment of a newly developed sensor, namely, CSCAT, for the period of 1 January to 31 December 2019 with respect to global buoys from 6 sources (NDBC, TAO/TRITON, PIRATA, RAMA, PMEL, and MNR). Only buoys located offshore were selected, and the time difference and spatial separation between CSCAT and buoys were limited to less than 30 min and 25 km, respectively. First, the data quality of the satellite and buoy observations were strictly controlled; for example, satellite data flagged for rain, ice and land were excluded. The measured height of the buoy was converted to the equivalent neutral wind at a height of 10 m, as observed by the CFOSAT. Second, the bias, RMSE, and R were selected as error statistics to analyze CSCAT winds in the ranges of 0-4 $ms^{-1}$ and 4-24 $ms^{-1}$ in different regions. It was found that CSCAT has good reliability in the wind speed range of 4-24 $ms^{-1}$. Globally, the RMSE of wind speed was slightly higher than 1 $ms^{-1}$, and the RMSE of wind direction was approximately 20°. The accuracy of CSCAT in the subtropics was significantly higher than that in the tropics. Finally, six buoys were used to evaluate the accuracy, including and excluding the surface currents, and the influence of ocean currents on wind vector retrieval was discussed. The effect of excluding the influence of ocean currents on the results depends mainly on the ratio of the surface current speed to the wind speed. For the six buoys in this study, the buoys (0°N, 110°W and 0°N, 140°W) in the tropical regions were greatly improved, and the RMSEs of wind speed and wind direction increased by approximately 0.1 $ms^{-1}$ and 2°, respectively. For the wind vector, the quality improvement is mainly focused on the zonal wind, and the RMSE of the zonal wind at these two sites increased by 0.2 $ms^{-1}$ and 0.3 $ms^{-1}$, respectively, while the corresponding meridional wind did not show significant improvement.

Although the performance of the scatterometer varied from region to region, considering the differences in time and distance between buoy measurements and satellite observations, the accuracy of CSCAT winds met the design quality requirements, especially the wind speed. In addition, the results show that the retrieval accuracy of CSCAT wind was reduced because of currents in the tropics, and the bias agreed well with the relationship between the current direction and wind direction. The major purpose of this paper is to show the basic uncertainties in CSCAT, which can help potential users understand existing errors. It is expected that the CSCAT products can not only be used in operational systems but also support fundamental research in physical oceanography and air-sea interactions. In addition, the joint observations of China's HY-2 satellites and the European Organization for the Exploitation of Meteorological Satellites MetOp satellites can better serve oceanic research and forecasting and can be used to generate higher-quality merged wind products to provide data support for marine disaster prevention and mitigation and climate change. The simultaneous observations of winds and waves over a large area by CFOSAT have unique application potential for studying the coupling process at the boundary between the atmosphere and waves and the effects of waves on scatterometer retrieval.

## Acknowledgments

This study is funded by the National Natural Science Foundation of China (42076016). The authors extend their thanks to the joint cruise team from the First Institute of Oceanography, Ministry of Natural Resources, China, and the Centre for Southern Hemisphere Oceans Research, Hobart, Tasmania, Australia. The authors also thank the buoy maintenance team from the South China Sea Bureau of Ministry of Natural Resources and South China Sea Institute of Oceanology, Chinese Academy of Sciences. The CFOSAT data and global buoy datasets from TAO/TRITON, RAMA, PIRATA, NDBC, and PMEL can be downloaded from http://osdds.nsoas.org.cn, https://www.pmel.noaa.gov/gtmba/data-access/disdel, https://www.ndbc.noaa.gov/data/l_stdmet, and https://www.pmel.noaa.gov/ocs/data/disdel, respectively. The authors appreciate the constructive comments and suggestions from the anonymous reviewers.

## References

Atlas, R., Hoffman, R. N., Ardizzone, J., Leidner, S. M., Jusem, J. C., Smith, D. K., & Gombos, D. (2011). A cross-calibrated, multiplatform ocean surface wind velocity product for meteorological and oceanographic applications. *Bulletin of the American Meteorological Society*, *92*(2), 157-174. https://doi.org/10.7289/V57942PP

Bentamy, A., Quilfen, Y., Queffeulou, P., & Cavanie, A. (1994). Calibration of the ERS-I scatterometer C-band model*(DRO OS-94-01)*. Brest, France: IFREMER.

Bonhoure, D., Rowe, E., Mariano, A. J., & Ryan, E. H. The South Equatorial Sys Current. Availabe online: https://oceancurrents.rsmas.miami.edu/atlantic/south-equatorial.html. (accessed on 14 Jan 2021).

Bourassa, M. A., Freilich, M. H., Legler, D. M., Liu, W. T., & O"Brien, J. J. (1997). Wind observations from new satellite and research vessels agree. *Eos Transactions American Geophysical Union*, *78*(51), 597. https://doi.org/10.1029/97EO00357

Bourassa, M. A., Bonekamp, H., Chang, P., Chelton, D., & Wentz, F. (2009). Remotely sensed winds and wind stresses for marine forecasting and ocean modeling. Paper presented at oceanobs'09: Sustained Ocean Observations and Information for Society, European Space Agency, Venice, Italy.

Brocca, L., Hasenauer, S., Lacava, T., Melone, F., Moramarco, T., Wagner, W., et al. (2011). Soil moisture estimation through ASCAT and AMSR-E sensors: An intercomparison and validation study across Europe. *Remote Sensing of Environment*, *115*(12), 3390-3408. https://doi.org/10.1016/j.rse.2011.08.003

Brodeau, L., Barnier, B., Gulev, S. K., & Woods, C. (2016). Climatologically significant effects of some approximations in the bulk parameterizations of turbulent air-sea fluxes. *Journal of Physical Oceanography*, *47*(1), 5-28. https://doi.org/10.1175/JPO-D-16-0169.1

Chelton, D. B., Freilich, M. H., & Johnson, J. R. (1989). Evaluation of Unambiguous Vector Winds from the Seasat Scatterometer. *Journal of Atmospheric and Oceanic Technology*, *6*(6), 1024-1039. https://doi.org/10.1175/1520-0426(1989)0062.0.CO;2

Chelton, D. B., & Freilich, M. H. (2005). Scatterometer-based assessment of 10-m wind analyses from the operational ECMWF and NCEP numerical weather prediction models. *Monthly Weather Review*, *133*(2), 409-429. https://doi.org/10.1175/MWR-2861.1

Chen, S., Rutgersson, A., Yin, X., Xu, Y., & Qiao, F. (2020). On the first observed wave-induced stress over the global ocean. *Journal of Geophysical Research: Oceans*, *125*(12), e2020JC016623. https://doi.org/10.1029/2020JC016623

Dawe, J. T., & Thompson, L. A. (2006). Effect of ocean surface currents on wind stress, heat flux, and wind power input to the ocean. *Geophysical Research Letters*, *33*(9), 179-212. https://doi.org/10.1029/2006GL025784

Dickinson, S., Kelly, K. A., Caruso, M. J., & Mcphaden, M. J. (2001). Comparisons between the TAO buoy and NASA scatterometer wind vectors. *Journal of Atmospheric and Oceanic Technology*, *18*(5), 799-806. https://doi.org/10.1175/1520-0426(2001)018<0799:CBTTBA>2.0.CO;2

Donelan, M. A., & Pierson, W. J. (1987). Radar scattering and equilibrium ranges in wind-generated waves with application to scatterometry. *Journal of Geophysical Research: Oceans*, *92*(C5), 4971-5029. https://doi.org/10.1029/JC092iC05p04971

Donguy, J.-R., & Meyers, G. (1996). Mean annual variation of transport of major currents in the tropical Pacific Ocean. *Deep Sea Research Part I: Oceanographic Research Papers*, *43*(7), 1105-1122. https://doi.org/10.1016/0967-0637(96)00047-7

Ebuchi, N. (1999). Statistical distribution of wind speeds and directions globally observed by NSCAT. *Journal of Geophysical Research: Oceans*, *104*(C5), 11393-11403. https://doi.org/10.1029/98JC02061

Ebuchi, N., Graber, H. C., & Caruso, M. J. (2002). Evaluation of wind vectors observed by QuikSCAT/SeaWinds using ocean buoy data. *Journal of Atmospheric and Oceanic Technology*, *19*(12), 2049–2062. https://doi.org/10.1175/1520-0426(2002)019<2049:EOWVOB>2.0.CO;2

Ekman, V. W. (1905). *On the influence of the earth's rotation on ocean currents*. Uppsala, Sweden: Arkiv for Matematik, Astronomi och Fysik.

Feng, M., Duan, Y., Wijffels, S., Hsu, J.-Y., Li, C., Wang, H., et al. (2020). Tracking air–sea exchange and upper-ocean variability in the Indonesian–Australian basin during the onset of the 2018/19 Australian summer monsoon. *Bulletin of the American Meteorological Society*, *101*(8), E1397-E1412. https://doi.org/10.1175/bams-d-19-0278.1

Freilich, M. H. (1997). Validation of vector magnitude datasets: Effects of random component errors. *Journal of Atmospheric and Oceanic Technology*, *14*(3), 695-703. https://doi.org/10.1175/1520-0426(1997)014<0695:VOVMDE>2.0.CO;2

Freitag, H. P., Ning, C., Berk, P. L., Dougherty, D. M., Marshall, R. F., Strick, J. M., & Zimmerman, D. K. (2016). ATLAS, T-Flex, BaiLong meteorological sensor comparison test report*(OAR PMEL-148)*. Seattle, WA, USA: NOAA/Pacific Marine Environmental Laboratory.

Gilhousen, D. B. (1987). A field evaluation of NDBC moored buoy winds. *Journal of Atmospheric and Oceanic Technology*, *4*(1), 94-104. https://doi.org/10.1175/1520-0426(1987)004<0094:AFEONM>2.0.CO;2

Huang, R. (2010). *Ocean circulation : wind-driven and thermohaline processes*. Cambridge, UK: Cambridge University Press.

Jourdan, D., & Gautier, C. (1995). Comparison between global latent heat flux computed from multisensor (SSM/I and AVHRR) and from in situ data. *Journal of Atmospheric and Oceanic Technology*, *12*(1), 46-72. https://doi.org/10.1175/1520-0426(1995)012<0046:CBGLHF>2.0.CO;2

Kelly, K. A., Dickinson, S., Mcphaden, M. J., & Johnson, G. C. (2001). Ocean currents evident in satellite wind data. *Geophysical Research Letters*, *28*(12), 2469-2472. https://doi.org/10.1029/2000GL012610

Kessler, W. S., S. E. Wijffels, S. Cravatte, N. Smith, & Authors, L. (2019). Second report of TPOS 2020*(GOOS-234)*.

KNMI. NSCAT-4 geophysical model function. Availabe online: https://scatterometer.knmi.nl/nscat_gmf (accessed on 27 Feb 2021).

Kumar, R., Chakraborty, A., Parekh, A., Sikhakolli, R., Gohil, B. S., & Kumar, A. S. K. (2013). Evaluation of Oceansat-2-derived ocean surface winds using observations from global buoys and other scatterometers. *IEEE Transactions on Geoscience and Remote Sensing*, *51*(5), 2571-2576. https://doi.org/10.1109/TGRS.2012.2214785

Lin, W., Dong, X., Portabella, M., Lang, S., He, Y., Yun, R., et al. (2019). A perspective on the performance of the CFOSAT rotating fan-beam scatterometer. *IEEE Transactions on Geoscience and Remote Sensing*, *57*(2), 627-639. https://doi.org/10.1109/TGRS.2018.2858852

Liu, W. T., Katsaros, K. B., & Businger, J. A. (1979). Bulk parameterization of air-sea exchanges of heat and water vapor including the molecular constraints at the interface. *Journal of the Atmospheric Sciences*, *36*(9), 1722-1735. https://doi.org/10.1175/1520-0469(1979)036<1722:BPOASE>2.0.CO;2

Liu, W. T., & Tang, W. Q. (1996). Equivalent neutral wind.*(JPL Publication 96–17)*. Pasadena, CA, USA: Jet Propulsion Laboratory.

Liu, Y., Lin, M., Jiang, X., Sun, X., & Song, X. (2021). A comparison of multiplatform wind products in the South China Sea during summer and autumn in 2019. *Journal of Oceanology and Limnology*. https://doi.org/10.1007/s00343-020-0207-2

Luo, J. J., Masson, S., Roeckner, E., Madec, G., & Yamagata, T. (2005). Reducing climatology bias in an ocean-atmosphere CGCM with improved coupling physics. *Journal of Climate*, *18*(13), 2344-2360. https://doi.org/10.1175/JCLI3404.1

NDBC. How are the station ID numbers created? Availabe online: https://www.ndbc.noaa.gov/staid.shtml (accessed on 14 Jan 2021).

NSOAS. CFOSAT Series. Availabe online: http://www.nsoas.org.cn/eng/ (accessed on 14 Jan 2021).

Pedlosky, J. (1987). *Geophysical fluid dynamics*. (2nd ed.). New York, USA: Springer.

Pollard, R. T., Rhines, P. B., & Thompson, R. O. R. Y. (1973). The deepening of the wind-Mixed layer. *Geophysical Fluid Dynamics*, *4*(4), 381-404. https://doi.org/10.1080/03091927208236105

Price, J. F., Weller, R. A., & Pinkel, R. (1986). Diurnal cycling: Observations and models of the upper ocean response to diurnal heating, cooling, and wind mixing. *Journal of Geophysical Research: Oceans*, *91*(C7). https://doi.org/10.1029/JC091iC07p08411

Price, J. F., Weller, R. A., & Schudlich, R. R. (1987). Wind-driven ocean currents and ekman transport. *Science*, *238*(4833), 1534-1538. https://doi.org/10.1126/science.238.4833.1534

Schmidt, K. M., Swart, S., Reason, C., & Nicholson, S.-A. (2017). Evaluation of satellite and reanalysis wind products with in situ wave glider wind observations in the Southern Ocean. *Journal of Atmospheric and Oceanic Technology*, *34*(12), 2551-2568. https://doi.org/10.1175/jtech-d-17-0079.1

Schott, F. A., & Mccreary, J. P. (2001). The monsoon circulation of the Indian Ocean. *Progress in Oceanography*, *51*(1), 1-123. https://doi.org/10.1016/S0079-6611(01)00083-0

Song, X. (2021). The importance of including sea surface current when estimating air-sea turbulent heat fluxes and wind stress in the Gulf Stream region. *Journal of Atmospheric and Oceanic Technology*, *38*, 119-138. https://doi.org/10.1175/JTECH-D-20-0094.1

Thorpe, S. A. (2004). Langmuir circulation. *Annual Review of Fluid Mechanics*, *36*(1), 55-79. https://doi.org/10.1146/annurev.fluid.36.052203.071431

Verspeek, J., Stoffelen, A., Portabella, M., Bonekamp, H., Anderson, C., & Saldana, J. F. (2010). Validation and calibration of ASCAT using CMOD5.n. *IEEE Transactions on Geoscience and Remote Sensing*, *48*(1), 386-395. https://doi.org/10.1109/TGRS.2009.2027896

Wang, L., Ding, Z., Zhang, L., & Yan, C. (2019). CFOSAT-1 realizes first joint observation of sea wind and waves. *Aerospace China*, *20*(01), 22-29.

Wang, Z., Stoffelen, A., Zou, J., Lin, W., Verhoef, A., Zhang, Y., et al. (2020). Validation of new sea surface wind products from scatterometers onboard the HY-2B and MetOp-C satellites. *IEEE Trans. Geosci. Remote Sensing 58*(6), 4387-4394. https://doi.org/10.1109/TGRS.2019.2963690

Wanninkhof, R. (1992). Relationship between wind speed and gas exchange over the ocean. *Journal of Geophysical Research: Oceans*, *97*(C5), 7373-7382. https://doi.org/10.1029/92JC00188

Wanninkhof, R., & Mcgillis, W. R. (1999). A cubic relationship between air-sea CO2 exchange and wind speed. *Geophysical Research Letters*, *26*(13), 1889-1892. https://doi.org/10.1029/1999GL900363

Xu, X., Dong, X., & Xie, Y. (2020). On-board wind scatterometry. *Remote Sensing*, *12*(7), 1216. https://doi.org/10.3390/rs12071216

Yu, L., & Jin, X. (2012). Buoy perspective of a high-resolution global ocean vector wind analysis constructed from passive radiometers and active scatterometers (1987–present). *Journal of Geophysical Research*, *117*(C11), 143–156. https://doi.org/10.1029/2012JC008069

Yu, Z., McCreary Jr, J. P., Kessler, W. S., & Kelly, K. A. (2000). Influence of equatorial dynamics on the pacific North Equatorial Countercurrent. *Journal of Physical Oceanography*, *30*(12), 3179-3190. https://doi.org/10.1175/1520-0485(2000)030<3179:IOEDOT>2.0.CO;2

Zhao, K., & Zhao, C. (2019). Evaluation of HY-2A scatterometer ocean surface wind data during 2012–2018. *Remote Sensing*, *11*(24), 2968-2889. https://doi.org/10.3390/rs11242968

Zhao, X., & Hou, Y. (2006). Analysis of ERS-2 scatterometer winds and wind-wave calculation for eastern China seas. *Chinese Journal of Oceanology and Limnology*, *24*(1), 69-75. https://doi.org/10.1007/BF02842777